Published in final edited form as:
Biomaterials. 2013 June ; 34(18): 4439–4451. doi:10.1016/j.biomaterials.2013.02.065.

MACROPHAGE FUNCTIONAL POLARIZATION (M1/M2) IN RESPONSE TO VARYING FIBER AND PORE DIMENSIONS OF ELECTROSPUN SCAFFOLDS

K. Garg[¥], **N.A. Pullen**[#,1], **C.A. Oskeritzian**[€,2], **J.J. Ryan**[#], and **G.L. Bowlin**[¥,*]

[¥]Department of Biomedical Engineering, Virginia Commonwealth University, Richmond, VA 23284, USA

[#]Department of Biology, Virginia Commonwealth University, Richmond, VA 23284, USA

[€]Department of Biochemistry and Molecular Biology, Virginia Commonwealth University, Richmond, VA 23298, USA

Abstract

In this study, we investigated the effect of fiber and pore size of an electrospun scaffold on the polarization of mouse bone marrow-derived macrophages (BMMΦs) towards regenerative (M2) or inflammatory (M1) phenotypes. BMMΦs were seeded on Polydioxanone (PDO) scaffolds electrospun from varying polymer concentrations (60, 100, and 140 mg/ml). Higher polymer concentrations yielded larger diameter fibers with larger pore sizes and porosity. BMMΦ cultured on these scaffolds showed a correlation between increasing fiber/pore size and increased expression of the M2 marker Arginase 1 (Arg1), along with decreased expression of the M1 marker inducible nitric oxide synthase (iNOS). Secretion of the angiogenic cytokines VEGF, TGF-β1 and bFGF was higher among cultures employing larger fiber/pore size scaffolds (140 mg/ml). Using a 3D *in vitro* angiogenesis bead assay, we have demonstrated that the M2-like profile of BMMΦ induced by the 140 mg/ml is functional. Furthermore, our results show that the pore size of a scaffold is a more critical regulator of the BMMΦ polarization compared to the fiber diameter. The study also shows a potential role for MyD88 in regulating M1 BMMΦ signaling on the large vs. small fiber/pore size PDO scaffold. These data are instructive for the rationale design of implantable prosthetics designed to promote *in situ* regeneration.

Keywords

Macrophages; electrospinning; polydioxanone; angiogenesis

[*]Corresponding Author. School of Engineering, Department of Biomedical Engineering, East Hall, Room E1254, 401W. Main St., P.O. Box 843067, Richmond, VA 23284-3067, USA. Tel.: +1 804 828 2592. glbowlin@vcu.edu (G.L. Bowlin).
[1]Present Address: Department of Biology, William Woods University, One University Avenue, Fulton, MO 65251, USA.
[2]Present Address: Department of Pathology, Microbiology and Immunology, University of South Carolina, School of Medicine, 6439 Garners Ferry Road, Columbia, SC 29208, USA.

1. Introduction

Tissue engineered biomaterials often induce an inflammatory reaction, also known as the foreign body response (FBR) after implantation. Upon exposure to implanted biomaterials, macrophages (MΦs) fuse into multinucleated giant cells called foreign-body giant cells (FBGCs), leading to fibrous encapsulation [1, 2]. However, MΦs are also essential for early remodeling processes. The phenotypic profile of MΦs as M1 or M2 following exposure to the biomaterial can dictate remodeling and angiogenesis [3, 4]. These processes are modulated via “cross-talk” between MΦs and other cells (e.g. endothelial cells), as well as factors within the local environment [5, 6]. This study aims to gather insight into MΦs response to electrospun PDO by identifying the MΦs phenotype (M1 or M2). In general, M1s or classically activated MΦs are pro-inflammatory and microbicidal, whereas M2s or alternatively activated MΦs are immunomodulatory, reparative, and poorly microbicidal [7–12]. The balance of these two phenotypes plays a critical role in the phagocytosis of pathogens, the clearance of apoptotic cells, and the remodeling of injured tissues. The actual MΦ phenotype is viewed as a continuum of functional states between these two opposing ends [13].

Recently M2s were further divided into M2a, M2b, and M2c based on their different roles in tissue remodeling. M2a phenotype is associated with Th2 responses, and arises in response to Interleukin (IL)-4 and IL-13. The M2b phenotype is induced by immune complexes as well as agonists of Toll-like Receptors (TLRs) or IL-1 receptors, and secretes high amounts of IL-10 but reduced IL-12. M2c phenotype is induced by IL-10 or glucocorticoids, produces elevated levels of IL-10 and Transforming Growth Factor-beta 1 (TGF-β1), and is associated with immune suppression and remodeling [13, 14]. In contrast, Interferon-gamma (INF-γ) or Tumor Necrosis Factor-alpha (TNF-α) primed MΦs are grouped as M1s. These MΦs have decreased phagocytic capability and (FcγR)II expression. M1s secrete pro-inflammatory cytokines, such as TNF-α, IL-1, IL-6, IL-12, and IL-23, possess anti-proliferative functions, and induce Th1 responses. In addition, M1s are also crucial in matrix destruction and tissue reorganization at injured tissues via the production of a variety of enzymes such as matrix metalloproteinases (MMPs), collagenase, elastase and hyaluronidase. This allows M1s to quickly migrate through injured tissues to clear pathogens and debris [13]. Mosser *et al.* suggested a spectrum of MΦ phenotypes and characterized MΦ populations based on three fundamental homeostatic activities: host defense, wound healing, and immune regulation. MΦ are grouped into three primary phenotypes: classically activated MΦ for microbicidal activity, wound-healing MΦ for tissue repair, and regulatory MΦ for anti-inflammatory activity [15].

Regradless, it is clear that MΦ phenotypes exhibit plasticity. Since prolonged M1 activation leads to tissue injury, M1s must transition to M2s to facilitate proper tissue remodeling after disinfecting and debriding a wound site. In a recent study of skin biopsies from human patients, gene expression was analyzed at early (Day 1–2) and late (Day 4–8) stages of cutaneous wound healing. It was observed that the early stage included a mix of M1 and M2 markers (11 M1 genes and 7 M2 genes) whereas the late stage demonstrated predominately M2 markers (1 M1 gene and 9 M2 genes) [16].

MΦ response to biomaterials is also dependent on their size. It has been shown that when foreign materials are < 10 μm, MΦ can effectively phagocytose them. On encountering larger foreign materials (10–100 μm) that cannot be engulfed by a single MΦ, mutltinucleated MΦs or FBGCs are formed by the fusion of multiple MΦs. These FBGCs then phagocytose and digest the foreign materials. When FBGCs encounter bulk materials that even they cannot effectively engulf, they undergo a process called “frustrated

phagocytosis". In this process MΦs release an array of substances such as cytokines, reactive oxygen species and proteinases in an attempt to degrade the implanted materials [2].

The impact of fiber size on the MΦ response has also been examined. A report showed that nanofibrous poly(L-lactic)(PLLA) scaffolds (fiber size ~ 0.6 μm) minimized the inflammatory response of RAW264.7 MΦs cell line when compared to films and microfibrous (fiber size ~ 1.6 μm) scaffolds. Histological evaluation demonstrated a higher number of FBGCs on the PLLA film than on the micro- and nanofibrous scaffolds. Scaffold pore size can also alter the MΦ response and subsequent angiogenic functions [10, 11]. Dr. Ratner and co-workers fabricated poly (2-hydroxyethyl methacrylate-co-methacrylic acid) (pHEMA-co-MAA) hydrogel scaffolds with parallel channels by polymer fiber templating. The cardiac implantation of these hydrogels with pore diameters of 30–40 μm showed maximum vascularization and minimal fibrotic response, coupled with an increased number of M2 phenotype MΦs [17].

Polydioxanone (PDO) is a colorless, crystalline, biodegradable polymer that was developed for biodegradable wound closure sutures. It exhibits high flexibility, higher strength retention, slower absorption rate, and lower inflammatory response as compared to poly(glycolide lactide) and poly(glycolic acid) [18]. PDO has been widely used for vascular tissue engineering applications [18–24]. Greisler *et al.* published results utilizing PDO absorbable vascular prosthetics in a rabbit aortic model of regeneration. The results showed no perigraft hematomas, myofibroblast migration, confluent EC lining and reduced thromobogenicity with PDO scaffolds [21]. In addition to the above mentioned properties, PDO was chosen for this study because when electrospun at a particular concentration, it produces scaffolds with a fairly uniform distribution of fiber sizes and pore sizes [18, 20]. Due to this limited variability with respect to fiber and pore dimensions, PDO provided an excellent model and allowed for clear interpretation of results.

While MΦ cell lines are useful and easy to manipulate, they are not functionally equivalent to primary MΦs [25]. We employed primary bone marrow-derived macrophages (BMMΦ) to examine the relationship between fiber size/pore size, MΦ phenotype and angiogenic functions. We hypothesized that differences in pore size and fiber sizes of electrospun PDO would modulate BMMΦ phenotype (M1/M2) and thus influence the BMMΦ mediated angiogenesis. We also investigated if BMMΦ signal differently when in contact with electrospun materials of different fiber/pore sizes. Finally, we analyzed the separate contributions of pore size and fiber size on M2 polarization. These data are instructive for the rationale design of implantable prosthetics designed to promote *in situ* regeneration.

2. Materials and Methods

2.1 Electrospinning of Polydioxanone (PDO) Polymer

PDO (Ethicon Inc.) was dissolved in 1,1,1,3,3,3-hexafluoro-2-propanol (TCI America) in concentrations of 60, 100 and 140 mg/ml. These solutions were then loaded into a Becton Dickinson syringe (5.0 ml) with an 18 gauge blunt tip needle and placed in a KD Scientific syringe pump to be dispensed at a rate of 6 ml/hr. Solutions were then electrospun onto a flat rotating stainless steel mandrel (2.5 cm wide × 10.2 cm long × 0.3 cm thick) to produce a flat sheet. All electrospinning was performed at an applied voltage of 23 kV, while the mandrel was rotated at a rate of 500 rpm and placed 12 cm away from the needle tip. The fiber size of the electrospun scaffold was measured by Image J software (NIH). The pore size, porosity and surface area to volume ratio of the scaffolds was measured using a method described by Soliman *et al.* [26]. Briefly, 10 mm disks of the electrospun scaffolds were weighed and subsequently immersed in 70% ethanol overnight with slight mechanical agitation. This was done to allow the ethanol to penetrate into the scaffold pores. The

surface of the samples was then blotted dry on a filter paper and weighed once more to determine the mass of the ethanol present within the scaffold. Measurements were made on five sample disks of each scaffold type. The density of ethanol is 0.789 g/mL and the density of PDO is 1.34 g/mL. The porosity (ε) was calculated as:

$$\varepsilon = \frac{V_{ETH}}{V_{ETH} + V_{PDO}}$$

where V_{ETH} is the volume of the intruded ethanol and was calculated as the ratio between the observed mass change after intrusion and ρ_{ETH}. V_{PDO} is the volume of PDO fibers and was calculated as the ratio between the dry scaffold mass before intrusion and the density of PDO (ρ_{PDO}). The pore-radius was calculated from the following equation:

$$r = \frac{\omega}{\ln\left(\frac{1}{\varepsilon}\right)}$$

where ω is the fiber size and ε is the scaffold porosity. The surface area to volume ratio of the scaffolds was calculated using the formulas given by Boland *et al.* [18]:

$$\text{Surface area to volume ratio} = \frac{2^{*}\pi^{*}r_f{}^{*}L}{V_{PDO}}$$

$$L = \frac{M_{PDO}}{\rho_{PDO}{}^{*}\pi^{*}r^2}$$

where L is the equivalent fiber length, r_f is the average fiber radius.

2.2 Endotoxin Content

The endotoxin content of the electrospun PDO was determined by the Limulus Amebocyte Lysate (LAL) kinetic chromogenic assay (Endochrome-K™, Charles River) following manufacturer's protocol. Briefly, 6 mm disks of PDO were incubated in endotoxin-free distilled water at 37°C for 24 h. Afterwards, samples (water) were collected under sterile conditions and transferred to endotoxin-free tubes. Endotoxin levels were quantified using the LAL kinetic chromogenic assay at 450 nm [27].

2.3 BMMΦ Isolation and Cytokine Secretion

C57BL/6 mice were euthanized and the bone marrow was isolated from the femurs/tibias. The harvested bone marrow was cultured overnight in complete RPMI (with 1% penicillin and streptomycin, L-glutamine, HEPES, sodium pyruvate, 10% FBS, and 30 ng/ml recombinant murine MΦ-colony stimulating factor (rmM-CSF)). Cells were cultured for 7 days in the presence of rmM-CSF (30 ng/ml). Macrophage differentiation was verified by flow cytometry, showing >96% CD68+ (data not shown). After maturation, the BMMΦ were divided into three different groups and stimulated for 48 hrs in the presence of either murine IL-4 and IL-13 (Peprotech, 20 ng/ml each) to polarize BMMΦ to an M2 phenotype or murine INF-γ (Peprotech, 20 ng/ml) to polarize the BMMΦ to an M1 phenotype. The INF-γ treated BMMΦ were washed and further treated with LPS (Sigma-Aldrich L6529, 100 ng/ml) for 18 hrs. Untreated BMMΦs constituted the naïve group (M0s). In the majority

of the experiments described in this study, the unstimulated BMMΦ (M0s) will be compared against pre-polarized M1s (serving as negative control) and pre-polarized M2s (serving as positive control).

2.4 Phenotype Marker Expression (Arginase and iNOS) and Cytokine Secretion

BMMΦs (10^6 cells) were seeded on tissue culture plates (TCP, 24 well plates) and on ethanol disinfected, PDO scaffolds (15 mm discs) made from varying polymer concentrations (60, 100, and 140 mg/ml). After 24 hrs, the cell lysates were analyzed for Arg1 and iNOS expression by Western blot. Cell seeded scaffolds were removed from the well plate and transferred to a micro-centrifuge tube, rinsed with PBS and lysed on ice in 50 μl of cell lysis buffer (Cell Signaling Technology) containing protease inhibitor (Roche). The extracts were vortexed vigorously 3 times at 5 min intervals. Lysates were centrifuged and the supernatants were obtained and stored at −20°C until needed. Protein concentration was determined by the Bradford method using Bio-Rad's protein assay reagent. Protein lysates were denatured by boiling in Laemmli sample buffer (4×) for 10 mins and subjected to SDS-PAGE. The proteins separated in the gel were transferred to a nitrocellulose membrane. The membrane was blocked with 5% nonfat dry milk in Tris –buffered saline containing 1% Tween-20 (TBST). The membrane was then briefly rinsed in TBST and incubated in the primary antibody solution (containing 5% BSA) overnight at 4°C. Membranes were immunoblotted with antibodies against Arginase 1 (Abcam, ab91279, dilution 1:3000) and iNOS (Abcam, ab15323, dilution 1:2500). After 4× washes in TBST, the membrane was incubated in horseradish peroxidase-conjugated secondary IgG antibody (in 5% non-fat dry milk) for 1h at room temperature. After 4× washes in TBST, chemiluminescence was detected using the ECL Western blotting detection reagent (Pierce).

Cytokine secretion was evaluated by seeding 500,000 BMMΦs (M0, M1 and M2) on ethanol disinfected, electrospun PDO (10 mm discs) in 48-well tissue culture plates. The supernatants were collected after 24 and 72 hrs to quantify pro-inflammatory mediators (TNF-α, IL-6) and wound-healing mediators (Vascular Endothelial Growth Factor (VEGF), TGF-β1 and basic fibroblast growth factor (bFGF)). Chemokines (macrophage inflammatory protein -1 alpha (MIP-1α) and macrophage chemotactic protein (MCP-1)) were quantified by ELISA. All ELISA kits were purchased from Peprotech except for bFGF (Abcam) and TGF-β1 (R&D Systems).

2.5 Histology

On Day 3 after samples were recovered for ELISA (Section 2.4), polymer discs of each condition were fixed in 10% formalin and embedded in paraffin blocks. Sections were transferred on to slides, which were then stained with hematoxylin and eosin (H&E) to evaluate BMMΦs infiltration.

2.6 Three Dimensional (3D) Angiogenesis Assay

In order to assess the angiogenic potential of BMMΦs, a 3D angiogenesis bead assay was performed following the method described by Chen *et al.* [28] using conditioned media from the BMMΦ:PDO interaction. The BMMΦ were isolated from the bone marrow of C57BL/6 mice and transformed into M0, M1 and M2 and seeded on 15 mm disks of ethanol disinfected, PDO scaffolds electrospun at 60, 100 and 140 mg/ml in 24 well plate at a concentration of a 10^6 cells/ml. The cell culture supernatants were collected on Day 1 and 3.

Dry Cytodex 3 microcarrier beads (Sigma Aldrich) were hydrated and autoclaved according to manufacturer's recommendations. Approximately 6 million mouse endothelial cells (ECs, ATCC) (passage 5) were mixed with Cytodex beads (~9000) in 25 ml of endothelial growth media (EGM, DMEM high glucose with 10% FBS, 1% penicillin and streptomycin) media

in a 50 ml tube and incubated at 5% CO_2 and 37°C for 4–5 hours with agitation every 30 mins to avoid clumping of the bead-cell suspension and to ensure uniform coating. The mixture was then transferred to a T-25 flask and incubated overnight to allow the excess cells not attached to the beads to attach to the flask. The next morning the beads were washed twice in Ca^{2+} and Mg^{2+} free PBS. A collagen solution was prepared by combining eight volumes of cold bovine collagen type I (3 mg/ml, PureCol®) with one volume of 10× PBS and one volume of sodium hydroxide (0.1N). The EC coated beads were suspended in this collagen solution and transferred to 24 well plates (500 μL/well). The plates were incubated at 37°C and 5% CO_2 for 15 min to allow collagen gel formation. The EC coated beads were cultured in 500 μL of either BMMΦ: PDO conditioned media, EGM with 3% FBS (negative control) or EGM with 20 ng/ml murine VEGF (Peprotech) as positive control.

2.7 Quantification of Angiogenesis

Each well containing the EC coated bead was digitally photographed under inverted microscopy at Day 6. A special grid (Figure 1) made by dividing a circle with radially oriented lines around 360 degrees with 10 degree intervals was used to quantify the percentage density of sprouts. This grid has been used in a previous study to quantify the migration of sprouts in a 3D matrix [29]. The digital photographs were transparently overlaid with the grid in Adobe Photoshop. The number of grid spaces with sprouts were counted and divided by the total number of grid spaces. The length of the sprout was calculated using the Image J software (NIH). The length of sprout was measured from the surface of the bead (L-r) using the segmented line tool in the Image J software. A sprout was defined as a structure originating from the microcarrier bead surface that was > 45 μm in length.

2.8 Role of MyD88 in M2 Polarization on PDO Scaffolds

To investigate the role of MyD88 in this phenotypic switch, BMMΦs were isolated from the bone marrow of both B6×129 wild type and MyD88 knockout (KO) mice (Jackson Laboratories). BMMΦ were isolated and transformed *in vitro* into M1 and M2 as described in section 2.3. The BMMΦ were cultured on 60 mg/ml and 140 mg/ml PDO scaffolds (10^6 / disc) and TCP for 24 hrs and Arg1 expression was analyzed by Western blot.

2.9 Comparison of Fiber size vs. Pore Size in BMMΦ Phenotype Modulation

In order to investigate which property of the PDO scaffolds plays an important role in BMMΦ phenotype modulation, the 60 mg/ml PDO scaffolds were made more porous and the 140 mg/ml PDO scaffolds were made less porous without significantly changing their fiber size. The 60 mg/ml PDO scaffold was made more porous using air-flow impedance electrospinning [30]. The set-up is depicted in Figure 2. Briefly, PDO (60 mg/ml) was loaded into a 3 mL plastic Becton Dickinson syringe with an 18 gauge tip needle and dispensed at a rate of 6 ml/h. The needle tip was subjected to +25kV with an air gap distance of 20 cm between the needle and the mandrel. The perforated mandrel contained 0.75 mm diameter holes laterally spaced 2.0 mm center to center distance, while the center to center longitudinal distance was 1.50 mm. The perforated mandrel was subjected to an air pressure of 100 kPa. On one end of the perforated mandrel, a luer lock was fitted and taped to the perforated mandrel using electrical tape. On the other end, a 3 mm diameter solid mandrel was inserted into the perforated mandrel and taped in place.

The 140 mg/ml PDO scaffold was made less porous by compressing the scaffolds. Briefly, PDO scaffold of 140 mg/ml was cut into flat rectangular sheets. The sheets were then placed in between two flat stainless steel blocks. This assembly was compressed to 5000 psi using a mechanical hydraulic press (Carver, Inc. Wabash, IN) and the pressure was held for one

minute. This method of compression collapsed the pores in the scaffold. This led to a decrease in the pore size of the scaffold from 14 μm to 9 μm without impacting the fiber size.

In vitro polarized M2 BMMΦs (10^6) as described above were seeded on 12 mm disks of 60 mg/ml ethanol disinfected, PDO scaffolds electrospun on solid and air-flow impedance mandrels or on regular and compressed 140 mg/ml PDO scaffolds, in 48 well plates. Cell lysates were collected after 24 hours and analyzed for Arg1 expression.

2.10 Statistical Analysis

Data are expressed as means ± standard deviation. Each experiment was done in triplicates and was reproduced at least twice. All statistical analysis of the data was based on a Kruskal-Wallis one-way analysis of variance on ranks and a Tukey-Kramer pairwise multiple comparison procedure (α=0.05) performed with JMP®IN 8 statistical software (SAS Institute). $P<0.05$ was considered statistically significantly different (*).

3. Results

3.1 Electrospun PDO Properties

It was observed that by increasing the polymer concentration of PDO, electrospun scaffolds of varying properties were obtained (Figure 3). Increasing the polymer concentration led to a linear increase in the fiber sizes, pore sizes and porosity but decreased the surface area to volume ratio. The statistical differences were only observed in the case of 60 mg/ml and 140 mg/ml scaffolds. The properties of 100 mg/ml and 140 mg/ml scaffolds were not statistically different from one another.

3.2 Endotoxin Content

Before proceeding with any experiments using MΦs, PDO scaffolds were assayed for bacterial contamination by evaluating endotoxin levels in scaffolds. The values for endotoxin content ranged from 0.03 – 0.09 EU/ml. Therefore, the highest endotoxin level for any scaffold was at least 12,000 times lower than the lowest amount used to activate BMMΦs (100 ng/ml of LPS corresponding to 1100 EU/ml) and well below the acceptable U.S. Pharmacopeia standard for clinical applications (<0.25 EU/ml). This study indicated that the PDO materials used in this study were endotoxin free [31].

3.3 Histological Evaluation

The histological evaluation (H&E staining) of PDO scaffolds showed greater BMMΦ (M0s and M2s) infiltration into the fibrous structures of larger fiber/pore size scaffold (Figure 4A). BMMΦ infiltration was quantified using Image J (Figure 4B). As expected, the results showed that with increasing fiber/pore sizes, BMMΦ infiltration of the scaffold cross-sectional area for M0s and M2s increased linearly. The M0s and M2s in the case of small fiber/pore size PDO (60 mg/ml) scaffold were found concentrated at the surface. The BMMΦ infiltration was statistically higher in the large fiber/pore size scaffold (140 mg/ml) when compared to the 60 mg/ml scaffold. However, in the case of M1s, greater infiltration was observed on the 60 mg/ml. This observation might be attributed to the release of MMPs and other matrix degrading proteolytic enzymes (such as collagenase, elastase and hylauronidase) secreted by the M1 phenotype MΦs [13]. It is known that M1s invade tissues by degrading and destroying it in an attempt to clear the tissue of pathogens and debris [13].

3.4 Arginase and iNOS Expression

The results indicated a correlation between Arg1 expression and increasing fiber/pore sizes in all BMMΦ groups (M0, M1 and M2) on Day 1 (Figures 5A and B). The expression of iNOS decreased with increasing fiber/pore sizes. Three pieces of data emerge from these results: (1) These results indicate that the larger fiber/pore sizes (140 mg/ml PDO scaffold, 14 μm pore size) polarize towards an M2 phenotype in naïve BMMΦ (M0s). (2) The larger fiber/pore sizes are able to induce statistically higher Arg1 expression. The expression of iNOS in M1 pre-polarized BMMΦ is downregulated by increasing fiber/pore size (Figures 5A and C). However, it should be noted that the statistical difference was only found between 100 mg/ml and 140 mg/ml PDO scaffold. (3) The pre-polarized M2 BMMΦs induce statistically higher Arg1 expression on the large fiber/pore sizes on Day 1.

On Day 3, it was observed that M0s were unable to maintain Arg1 expression (Figure 6). However, M1 and M2s were able to maintain Arg1 expression. Similar to day 1, the larger fiber/pore sizes induced statistically higher Arg1 by M1s on Day 3. The Arg1 expression level by M2s was maintained on the large fiber/pore size. It was also observed that the M2s on the small fiber/pore size PDO increased their Arg1 production on Day 3 compared to Day 1. The expression of iNOS was totally abolished by Day 3 on all fiber/pore sizes of PDO.

3.5 BMMΦ Mediator Secretion

The production of cytokines and growth factors characteristic of both M1 and M2 phenotypes was quantified on Days 1 and 3. The levels of TNF-α, IL-6 (indicative of M1 phenoype) and growth factors associated with the M2 phenotype (VEGF, basic fibroblast growth factor (bFGF), TGF-β1) were measured by ELISA and normalized to the total protein content.

The levels of TNF-α are shown in Figure 7A. The highest levels of TNF-α were produced from the M1 phenotype BMMΦ (~ 300 times greater compared to M0s and M2s). The levels of TNF-α were not found to be significantly different between PDO scaffolds of different fiber/pore sizes. TNF-α levels decreased on Day 3 and trended lower on the 140 mg/ml scaffold.

The quantification of IL-6 cytokine is shown in Figure 7B. IL-6 was also produced in highest quantities by M1 phenotype BMMΦs. Similar to TNF-α, the levels of IL-6 were not downregulated by the large fiber/pore size PDO. IL-6 levels were unaffected by different fiber/pore sizes on either Day 1 or 3.

The levels of VEGF by BMMΦ are shown in Figure 7C. In the case of M0s, the production of VEGF was significantly higher on the larger fiber/pore size PDO. Continuing to look at M0s, it was observed that compared to Day 1, the level of VEGF on the 60 mg/ml scaffold were much lower on Day 3 indicating that the 60 mg/ml scaffold is unable to maintain the expression of VEGF. In contrast, the level of VEGF on the 140 mg/ml scaffold increased on Day 3 compared to Day 1 indicating sustained expression of VEGF on the 140 mg/ml scaffold. In the case of M1s and M2s, no differences with respect to fiber/pore sizes were noted.

TGF-β1 is secreted as a complex with latency associated peptide (LAP). In order to quantify the amount of TGF-β1 released, it must be released from LAP by utilizing acidic conditions that denature the LAP and free TGF-β1 from the complex [32]. Hence, the cell culture supernatants were acid-activated as per manufacturer's instructions prior to the TGF-β1 ELISA (Figure 7D). Comparable levels of TGF-β1 were produced by all three BMMΦ phenotypes; M0s, M1s and M2s. The TGF-β1 expression was maintained until Day 3. The levels of TGF-β1 increased with increasing fiber/pore sizes in M0s, M1s and M2s. The

production of TGF-β1 was statistically higher on the 140 mg/ml scaffold compared to the 60 mg/ml scaffold on Day 1 in the case of M0s and on both Day 1 and 3 in the case of M1s and M2s.

The quantification of bFGF is shown in Figure 7E. Just like the two other angiogenic growth factors VEGF and TGF-β1, bFGF was also produced in comparable amounts by BMMΦ of all three phenotypes; M0s, M1s and M2s. The production of bFGF was statistically higher on the 140 mg/ml scaffold compared to the 60 mg/ml scaffold on Day 1 in the case of M0s and M1s and on Day 3 in the case of M2s.

The expression of two chemokines: MIP-1α and MCP-1 is shown in Figure 7F and 7G respectively. The levels of MIP-1α were much higher in M0s compared to M1s and M2s. The production of MIP-1α was statistically higher on the larger fiber/pore size scaffold (140 mg/ml) compared to the 60 mg/ml scaffold in the case of M0s, M1s and M2s. The levels of MCP-1 were statistically higher on the 140 mg/ml PDO scaffold compared to the 60 mg/ml scaffold in the case of M1s on Day 1.

3.6 Angiogenic Potential of Macrophages of PDO Scaffolds

In order to assess the angiogenic potential of BMMΦs cultured on PDO scaffolds, a 3D angiogenesis bead assay was performed using conditioned media from the BMMΦ:PDO interaction. The results of the 3D bead assay are shown in Figure 8. A representative image of each condition done in triplicate is shown. In all cases (M0s, M1s and M2s), the images showed greater sprouting from the conditioned media from BMMΦ cultured on the larger fiber/pore size PDO (Figure 8A). Angiogenesis was measured by quantification of the average sprout length and the percentage density (Figure 8B and C). The average sprout length induced by M0s on the larger fiber/pore size (140 mg/ml) was statistically higher when compared to smaller fiber/pore sizes (100 mg/ml and 60 mg/ml PDO scaffolds). No sprouting was observed from the conditioned media of M0s cultured on the 60 mg/ml scaffold. The sprout length in the case of M0s cultured on the 140 mg/ml scaffold was statistically higher than all other samples tested except for the M2s cultured on the 140 mg/ml scaffold. This result shows that a naïve BMMΦ (M0) cultured on the 140 mg/ml scaffold possesses angiogenic capacity similar to a pre-polarized M2. The sprout lengths induced by M1s were not different across different fiber/pore sizes. In the case of M2s, the sprout length induced by the conditioned media from 140 mg/ml scaffold was statistically higher compared to the 60 mg/ml scaffold. Overall it was observed that M0s induced a ~200 fold higher and M2s induced a ~2 fold higher length of sprout from the 140 mg/ml compared to the 60 mg/ml PDO scaffolds.

The quantification of the percentage density of sprouts is shown in Figure 8C. It was observed that significantly higher density of sprouts was induced by BMMΦs (M0s, M1s and M2s) cultured on the larger fiber/pore sizes. Compared to the 60 mg/ml scaffolds, the 140 mg/ml scaffolds induced a 94 fold higher density of sprouts from M0s, 7 fold higher density of sprouts from M1s and 17 fold higher density of sprouts from M2s. Therefore, these studies show that the larger fiber/pore size PDO scaffold has greater potential for BMMΦ mediated angiogenesis compared to the 60 mg/ml scaffold.

The positive control used in this assay was 20 ng/ml VEGF. It should be noted that BMMΦ conditioned media (especially in the case of 140 mg/ml scaffold) produced greater average length of sprouts and higher percentage density of sprouts compared to the positive control. This can be attributed to the fact that BMMΦ conditioned media contains many growth factors besides VEGF (such as TGF-β1 and bFGF) which also play crucial roles in the process of angiogenesis. Therefore, it is not surprising that their combined effects produced greater sprouting than VEGF alone.

3.7 Role of MyD88 in Arginase Production on PDO Scaffolds

In a recent study, it was demonstrated that dendritic cells can sense polymers through a mechanism involving multiple TLR/MyD88-dependent pathways (TLR-2, 4, 6) [27]. We hypothesized that PDO scaffolds activate BMMΦs via TLRs. All TLRs signal through myeloid differentiation factor 88 (MyD88) except TLR-3 and TLR-4. TLR-4 can signal the presence of lipopolysaccharide (LPS) through either MyD88-dependent or MyD88-independent mechanisms.

In this study, we investigated whether PDO scaffolds of different fiber and pore sizes triggers differential signaling pathways in BMMΦs. The MyD88 knockout and wild-type (WT) M0s and M2s expressed similar levels of Arg1 on both 60 mg/ml and 140 mg/ml PDO scaffolds. The only difference was observed in the case of M1s cultured on the 140 mg/ml scaffold (Figure 9). The MyD88 knockout M1s showed severely impaired ability to express Arg1 on the 140 mg/ml scaffold when compared to the WT M1s. No differences were observed in MyD88 knockout and WT M1s cultured on the 60 mg/ml scaffold. This indicates that scaffolds with large and small fiber/pore sizes signal to M1s differently. The 140 mg/ml PDO scaffold signal to M1s through a MyD88-dependant mechanism whereas, 60 mg/ml PDO scaffold signals through a MyD88-independent mechanism. This result indicates a potential role for MyD88 in regulating M1 BMMΦ signaling on the large vs. small fiber/pore size PDO scaffold.

3.8 Comparison of Fiber size vs. PoreSize in BMMΦ Phenotype Modulation

During the electrospinning process, as fibers are deposited onto the perforated mandrel, pressurized air emanating from the mandrel perforations is introduced into the developing fibrous structure causing the fibers near the mandrel perforations to be less dense, creating regions of increased scaffold porosity. In contrast, fibers deposited on solid, non-perforated sections of the mandrel (e.g. located between and adjacent to the perforations) are, in comparison, densely packed. The scaffold thus contains regions in which the fibers are porous and regions in which the fibers are densely packed, all within a single contiguous, seamless structure prepared during a single deposition event, thus not requiring multiple deposition steps and/or processing steps [30]. The properties of scaffolds created on solid vs. perforated mandrels are shown in Figure 10. The air-flow impedance method created a statistically significant increase in the pore size and porosity of the scaffold but did not impact the fiber size and the surface area to volume ratio.

In vitro pre-polarized M2 BMMΦ, as previously described, were seeded on the 60 mg/ml PDO scaffolds (12 mm disks) created by traditional and air-flow impedance electrospinning methods at a density of 10^6 cells/well in 48 well plates. The cell lysates were collected after 24 hours and analyzed by Western blot for Arg1 expression. The analysis is shown in Figure 11. Compared to the solid mandrel, the air flow mandrel showed higher expression of Arg1 on M2s.

The properties of the compressed 140 mg/ml scaffold compared to the normal 140 mg/ml scaffold is shown in Figure 12. The Arg1 expression by M2s was reduced on the compressed 140 mg/ml scaffold compared to the normal 140 mg/ml scaffold (Figure 13). These results show that pore size is a more crucial regulator of the M2 phenotype compared to the fiber size.

4. Discussion

It has been shown by Greisler *et al.* [21, 33–36], Valentin *et al.* [37], Roh *et al.* [38], and Brown *et al.* [4] that macrophages play a key role in the success and potential failure of any biomaterial. Recognition of the predominant MΦ phenotypic profile can provide a tool by

which a tissue regenerative outcome can be predicted and possibly promoted [4]. In the present study, we examined the effects of fiber/pore size of an electrospun scaffold on MΦ polarization. By comparing naïve unstimulated M0s to pre-polarized M1 (negative control) and M2s (positive control) we have demonstrated that increased fiber/pore size shifts the MΦ phenotype to a more M2, tissue regenerative phenotype *in vitro*, as evidenced by increased Arg1, TGF-β1, VEGF, bFGF expression. Our objective was to discover conditions promoting an M2 phenotype that can function most effectively at tissue remodelling and angiogenesis. Such a functional M2 phenotype is likely to promote healing and integration of the biomaterial with the host tissue to enhance tissue regeneration. Using the 3D angiogenesis bead assay, we have shown that the BMMΦs of M2 phenotype are functional and can support angiogenesis. Most importantly, we have shown that a naïve BMMΦ (M0) when cultured on the 140 mg/ml scaffold not only acquires a more M2-like phenotype but is also as angiogenic as a pre-polarized M2. Therefore, this study shows that naïve BMMΦs acquire a functional M2-like phenotype when in contact with the bigger fiber/pore size scaffold.

The study indicates a potential role for MyD88 in regulating M1 BMMΦ signaling on the large vs. small fiber/pore size PDO scaffold. Future work will include further understanding of the signalling mechanism through which the BMMΦs sense and interact with electrospun polymers.

The impact of fiber size on MΦ activation has been studied previously [39, 40]. In the process of electrospinning the fiber and pore dimensions of a scaffold are largely dependent on the concentration of the polymer used. Both fiber and pore dimensions increase linearly with concentration [18]. Therefore, the analysis of separate contributions of fiber and pore size to MΦ response has not been done previously. The 60 mg/ml and 140 mg/ml PDO scaffolds differ remarkably in both pore size and fiber size. We have shown that BMMΦ are polarized towards a more M2-like phenotype on the 140 mg/ml scaffold. However, whether this result was because of the fiber size or the pore size remained unclear. To investigate this we designed a more porous 60 mg/ml scaffold using the air-flow impedance method. The 140 mg/ml PDO scaffold was made less porous by compressing it using a hydraulic press. Using these methods the fiber sizes of the two scaffolds remained constant but the pore size and the overall porosity of the scaffolds changed. The fact that we were able to modulate the Arg1 expression in the M2s by using scaffolds of the same fiber size but different pore sizes indicates that compared to the fiber size, pore size is a more crucial regulator of Arg1 expression and BMMΦ phenotype modulation towards an M2 phenotype.

Pore size has always been a crucial property of tissue engineering scaffolds and a key determinant of a scaffold's success through their influence on cell infiltration, nutrient/oxygen exchange, and angiogenesis [41, 42]. We speculate that in scaffolds with large pores, the MΦ are able to infiltrate more easily, which is supported by microscopic analysis of the scaffolds (Figure 4). Once inside, they are likely to orient themselves in the three-dimensional space and acquire a more natural and spread-out morphology. These micro-environmental cues may direct them to acquire the natural homeostatic tissue reparative roles performed by the M2s in the native tissues. In contrast, MΦ encountering scaffolds with smaller pores are largely concentrated on the surface of the scaffold unable to infiltrate. In an attempt to invade they may undergo "frustrated phagocytosis" and acquire tissue destructive roles which are typically associated with the M1s [17, 43].

Our data and the proposed hypotheses should set the stage for new *in vivo* research avenues aimed at evaluating biomaterials characteristics in relation to the MΦ phenotype. Future work may also include the evaluations of several other chemical and physical properties of a biomaterial that may be responsible for variations in the phenotypic profile of the MΦs. The

study presented here illustrates the MΦ responses in the early stages of inflammation (1–3 days). Studies that evaluate MΦ responses in the delayed stages of inflammation (7–14 days) may provide further insight into the biomaterial healing process.

The authors believe that the results of this study can be extrapolated to predict MΦ responses to other biomaterials as well. This study correlates material architecture with MΦ phenotypic responses and provides guidance for the design of biomaterials that promote angiogenesis and tissue regeneration without any undesirable immune responses.

5. Conclusion

In this study we have demonstrated that by varying the fiber and pore dimensions of an electrospun scaffold, the BMMΦ phenotype can be modulated. BMMΦ acquire a more tissue regenerative M2 phenotype on scaffolds with larger fiber and pore dimensions as evidenced by the increased production of Arg1, VEGF, bFGF and TGF-β1. We further demonstrated that these BMMΦs of M2 phenotype are functional and support angiogenesis and that the naïve BMMΦs acquire a functional M2-like phenotype when in contact with the bigger fiber/pore size scaffold. We have also shown that the scaffolds with different fiber/pore sizes signal to the BMMΦs differently and have identified MyD88 to be a key component involved in the signaling mechanism. Most importantly, we have shown that compared to the fiber size, pore size of a scaffold is a more critical regulator of the BMMΦ phenotype modulation towards an M2 phenotype. These data are instructive for the design and engineering of biomaterials that can promote in situ angiogenesis and tissue regeneration.

Acknowledgments

This research was supported by NIH 1R01AI059638 (J.J.R.) and the Louis and Ruth Harris Exceptional Scholar Professorship (G.L.B.).

References

1. Anderson JM. Biological Response to Materials. Annual Review of Materials Research. 2001; 31:81–110.
2. Anderson JM, Rodriguez A, Chang DT. Foreign body reaction to biomaterials. Semin Immunol. 2008; 20(2):86–100. [PubMed: 18162407]
3. Brown BN, Ratner BD, Goodman SB, Amar S, Badylak SF. Macrophage polarization: an opportunity for improved outcomes in biomaterials and regenerative medicine. Biomaterials. 2012; 33(15):3792–3802. [PubMed: 22386919]
4. Brown BN, Valentin JE, Stewart-Akers AM, McCabe GP, Badylak SF. Macrophage phenotype and remodeling outcomes in response to biologic scaffolds with and without a cellular component. Biomaterials. 2009; 30(8):1482–1491. [PubMed: 19121538]
5. Biswas SK, Mantovani A. Macrophage plasticity and interaction with lymphocyte subsets: cancer as a paradigm. Nat Immunol. 2010; 11(10):889–896. [PubMed: 20856220]
6. Stout RD, Jiang C, Matta B, Tietzel I, Watkins SK, Suttles J. Macrophages sequentially change their functional phenotype in response to changes in microenvironmental influences. J Immunol. 2005; 175(1):342–349. [PubMed: 15972667]
7. Fairweather D, Cihakova D. Alternatively activated macrophages in infection and autoimmunity. J Autoimmun. 2009; 33(3–4):222–230. [PubMed: 19819674]
8. Gordon S. Alternative activation of macrophages. Nat Rev Immunol. 2003; 3(1):23–35. [PubMed: 12511873]
9. Gordon S, Martinez FO. Alternative activation of macrophages: mechanism and functions. Immunity. 2010; 32(5):593–604. [PubMed: 20510870]

10. Martinez FO, Helming L, Gordon S. Alternative activation of macrophages: an immunologic functional perspective. Annu Rev Immunol. 2009; 27:451–483. [PubMed: 19105661]
11. Varin A, Gordon S. Alternative activation of macrophages: immune function and cellular biology. Immunobiology. 2009; 214(7):630–641. [PubMed: 19264378]
12. Galli SJ, Borregaard N, Wynn TA. Phenotypic and functional plasticity of cells of innate immunity: macrophages, mast cells and neutrophils. Nat Immunol. 2011; 12(11):1035–1044. [PubMed: 22012443]
13. Kou PM, Babensee JE. Macrophage and dendritic cell phenotypic diversity in the context of biomaterials. J Biomed Mater Res A. 2011; 96(1):239–260. [PubMed: 21105173]
14. Mantovani A, Sica A, Sozzani S, Allavena P, Vecchi A, Locati M. The chemokine system in diverse forms of macrophage activation and polarization. Trends Immunol. 2004; 25(12):677–686. [PubMed: 15530839]
15. Mosser DM, Edwards JP. Exploring the full spectrum of macrophage activation. Nat Rev Immunol. 2008; 8(12):958–969. [PubMed: 19029990]
16. Deonarine K, Panelli MC, Stashower ME, Jin P, Smith K, Slade HB, et al. Gene expression profiling of cutaneous wound healing. J Transl Med. 2007; 5:11. [PubMed: 17313672]
17. Madden LR, Mortisen DJ, Sussman EM, Dupras SK, Fugate JA, Cuy JL, et al. Proangiogenic scaffolds as functional templates for cardiac tissue engineering. Proc Natl Acad Sci U S A. 2010; 107(34):15211–15216. [PubMed: 20696917]
18. Boland ED, Coleman BD, Barnes CP, Simpson DG, Wnek GE, Bowlin GL. Electrospinning polydioxanone for biomedical applications. Acta Biomater. 2005; 1(1):115–123. [PubMed: 16701785]
19. Garg K, Ryan JJ, Bowlin GL. Modulation of mast cell adhesion, proliferation, and cytokine secretion on electrospun bioresorbable vascular grafts. J Biomed Mater Res A. 2011; 97(4):405–413. [PubMed: 21472976]
20. Garg K, Sell SA, Madurantakam P, Bowlin GL. Angiogenic potential of human macrophages on electrospun bioresorbable vascular grafts. Biomed Mater. 2009; 4(3) 031001.
21. Greisler HP, Ellinger J, Schwarcz TH, Golan J, Raymond RM, Kim DU. Arterial regeneration over polydioxanone prostheses in the rabbit. Arch Surg. 1987; 122(6):715–721. [PubMed: 3107517]
22. Greisler HP, Endean ED, Klosak JJ, Ellinger J, Dennis JW, Buttle K, et al. Polyglactin 910/ polydioxanone bicomponent totally resorbable vascular prostheses. J Vasc Surg. 1988; 7(5):697–705. [PubMed: 3130496]
23. McClure MJ, Sell SA, Ayres CE, Simpson DG, Bowlin GL. Electrospinning-aligned and random polydioxanone-polycaprolactone-silk fibroin-blended scaffolds: geometry for a vascular matrix. Biomed Mater. 2009; 4(5) 055010.
24. Sell SA, McClure MJ, Barnes CP, Knapp DC, Walpoth BH, Simpson DG, et al. Electrospun polydioxanone-elastin blends: potential for bioresorbable vascular grafts. Biomed Mater. 2006; 1(2):72–80. [PubMed: 18460759]
25. Chamberlain LM, Godek ML, Gonzalez-Juarrero M, Grainger DW. Phenotypic non-equivalence of murine (monocyte-) macrophage cells in biomaterial and inflammatory models. J Biomed Mater Res A. 2009; 88(4):858–871. [PubMed: 18357567]
26. Soliman S, Sant S, Nichol JW, Khabiry M, Traversa E, Khademhosseini A. Controlling the porosity of fibrous scaffolds by modulating the fiber diameter and packing density. J Biomed Mater Res A. 2011; 96(3):566–574. [PubMed: 21254388]
27. Shokouhi B, Coban C, Hasirci V, Aydin E, Dhanasingh A, Shi N, et al. The role of multiple toll-like receptor signalling cascades on interactions between biomedical polymers and dendritic cells. Biomaterials. 2010; 31(22):5759–5771. [PubMed: 20452017]
28. Chen Z, Htay A, Dos Santos W, Gillies GT, Fillmore HL, Sholley MM, et al. In vitro angiogenesis by human umbilical vein endothelial cells (HUVEC) induced by three-dimensional co-culture with glioblastoma cells. J Neurooncol. 2009; 92(2):121–128. [PubMed: 19039523]
29. Vernon RB, Sage EH. A novel, quantitative model for study of endothelial cell migration and sprout formation within three-dimensional collagen matrices. Microvasc Res. 1999; 57(2):118–133. [PubMed: 10049660]

30. McClure MJ, Wolfe PS, Simpson DG, Sell SA, Bowlin GL. The use of air-flow impedance to control fiber deposition patterns during electrospinning. Biomaterials. 2011; 33(3):771–779. [PubMed: 22054536]

31. United States Pharmacopeial Convention; 2009. Rockville, MD: 2009. General chapter <85> Bacterial Endotoxins Test, US Pharmacopeia 31 - National Formulary 26. 2009.

32. Lyons RM, Keski-Oja J, Moses HL. Proteolytic activation of latent transforming growth factor-beta from fibroblast-conditioned medium. J Cell Biol. 1988; 106(5):1659–1665. [PubMed: 2967299]

33. Greisler H. Macrophage-biomaterial interactions with bioresorbable vascular prostheses. ASAIO Trans. 1988; 34(4):1051–1059. [PubMed: 3064788]

34. Greisler HP, Dennis JW, Endean ED, Ellinger J, Buttle KF, Kim DU. Derivation of neointima in vascular grafts. Circulation. 1988; 78(3 Pt 2):I6–I12. [PubMed: 2970347]

35. Greisler HP, Dennis JW, Endean ED, Ellinger J, Friesel R, Burgess W. Macrophage/biomaterial interactions: the stimulation of endothelialization. J Vasc Surg. 1989; 9(4):588–593. [PubMed: 2523491]

36. Greisler HP, Tattersall CW, Klosak JJ, Cabusao EA, Garfield JD, Kim DU. Partially bioresorbable vascular grafts in dogs. Surgery. 1991; 110(4):645–654. discussion 654–645. [PubMed: 1833846]

37. Valentin JE, Stewart-Akers AM, Gilbert TW, Badylak SF. Macrophage participation in the degradation and remodeling of extracellular matrix scaffolds. Tissue Eng Part A. 2009; 15(7): 1687–1694. [PubMed: 19125644]

38. Roh JD, Nelson GN, Brennan MP, Mirensky TL, Yi T, Hazlett TF, et al. Small-diameter biodegradable scaffolds for functional vascular tissue engineering in the mouse model. Biomaterials. 2008; 29(10):1454–1463. [PubMed: 18164056]

39. Saino E, Focarete ML, Gualandi C, Emanuele E, Cornaglia AI, Imbriani M, et al. Effect of electrospun fiber diameter and alignment on macrophage activation and secretion of proinflammatory cytokines and chemokines. Biomacromolecules. 2011; 12(5):1900–1911. [PubMed: 21417396]

40. Sanders JE, Stiles CE, Hayes CL. Tissue response to single-polymer fibers of varying diameters: evaluation of fibrous encapsulation and macrophage density. J Biomed Mater Res. 2000; 52(1): 231–237. [PubMed: 10906696]

41. Yannas IV, Lee E, Orgill DP, Skrabut EM, Murphy GF. Synthesis and characterization of a model extracellular matrix that induces partial regeneration of adult mammalian skin. Proc Natl Acad Sci U S A. 1989; 86(3):933–937. [PubMed: 2915988]

42. Dagalakis N, Flink J, Stasikelis P, Burke JF, Yannas IV. Design of an artificial skin. Part III. Control of pore structure. J Biomed Mater Res. 1980; 14(4):511–528. [PubMed: 7400201]

43. Ratner BD, Bryant SJ. Biomaterials: where we have been and where we are going. Annu Rev Biomed Eng. 2004; 6:41–75. [PubMed: 15255762]

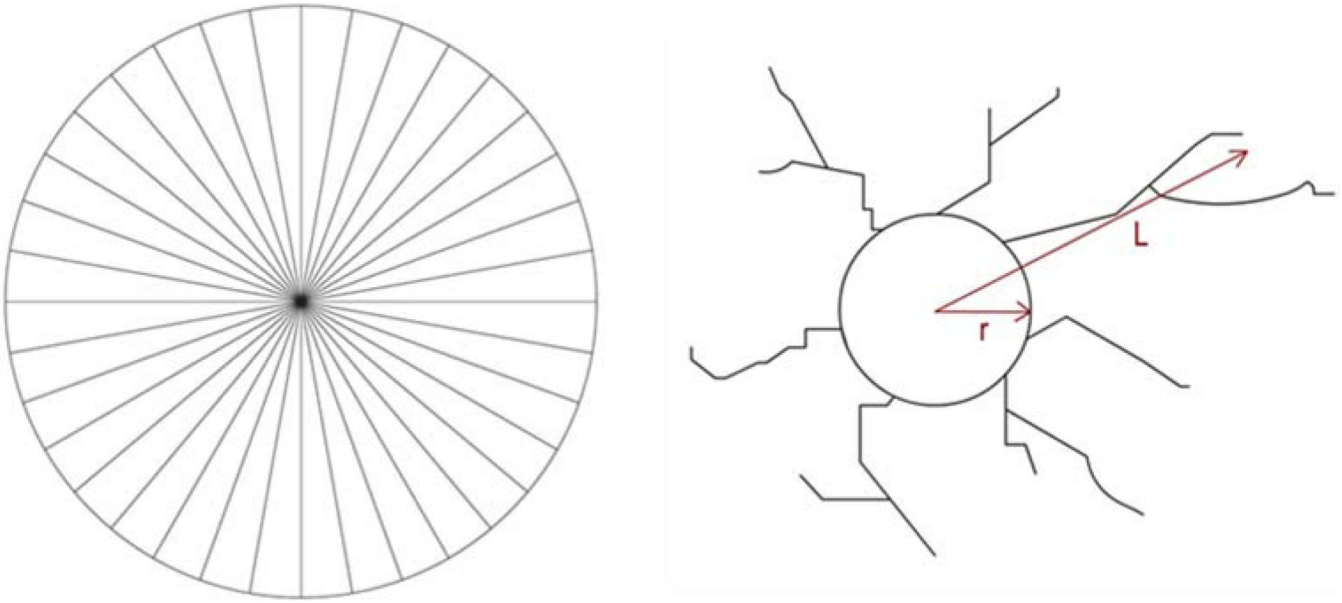

Figure 1.
Grid for quantification of angiogenesis (left) and diagram showing how the length of sprout (L-r) was calculated (right).

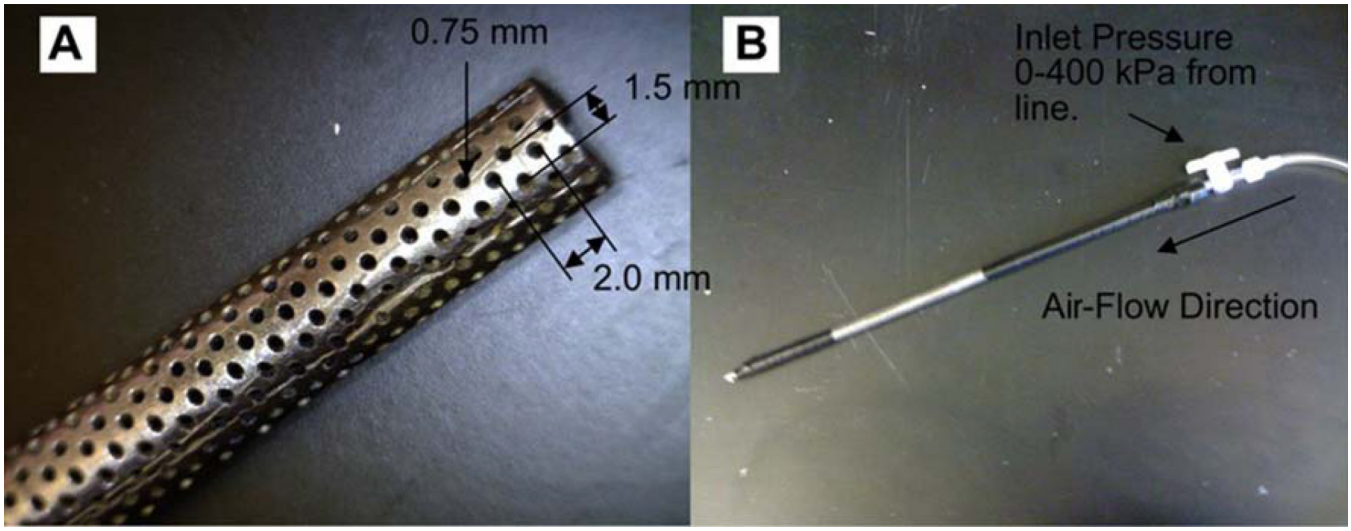

Figure 2.
(A) Perforated mandrel used for electrospinning, (B) mandrel set up with air line connected [13].

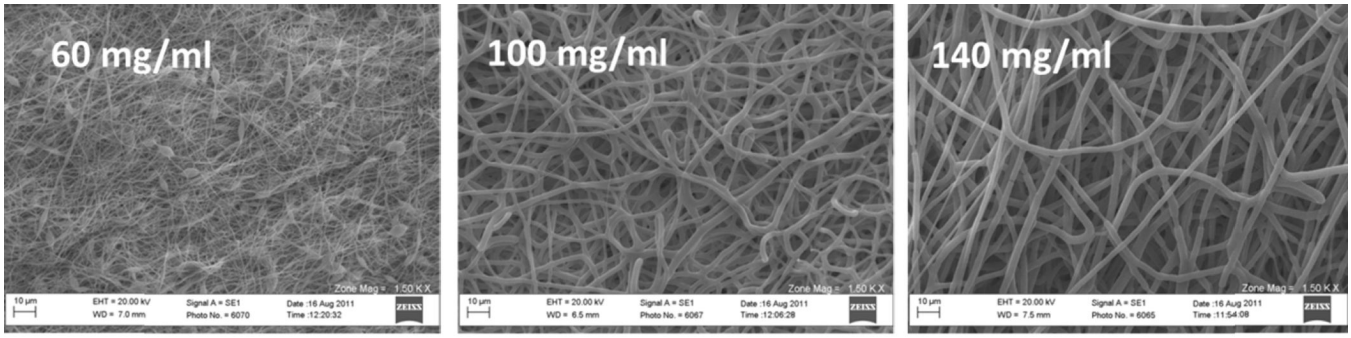

Concentration (mg/ml)	Pore Radius (μm)	Fiber Diameter (μm)	Surface Area to Volume Ratio (m^2/cm^3)	Porosity (%)
60	0.96 ± 0.09	0.35 ± 0.2	11.4	69.4 ± 2.33
100	10.57 ± 0.72	2.2 ± 0.1	1.8	81.16 ± 1.13
140	14.73 ± 0.62	2.8 ± 0.5	1.4	82.67 ± 0.703

Figure 3.
SEM micrographs demonstrating the architecture of the scaffolds tested along with the corresponding physical characteristics (pore radius, fiber diameter, surface-area-to-volume ratio, and porosity) determined for each group.

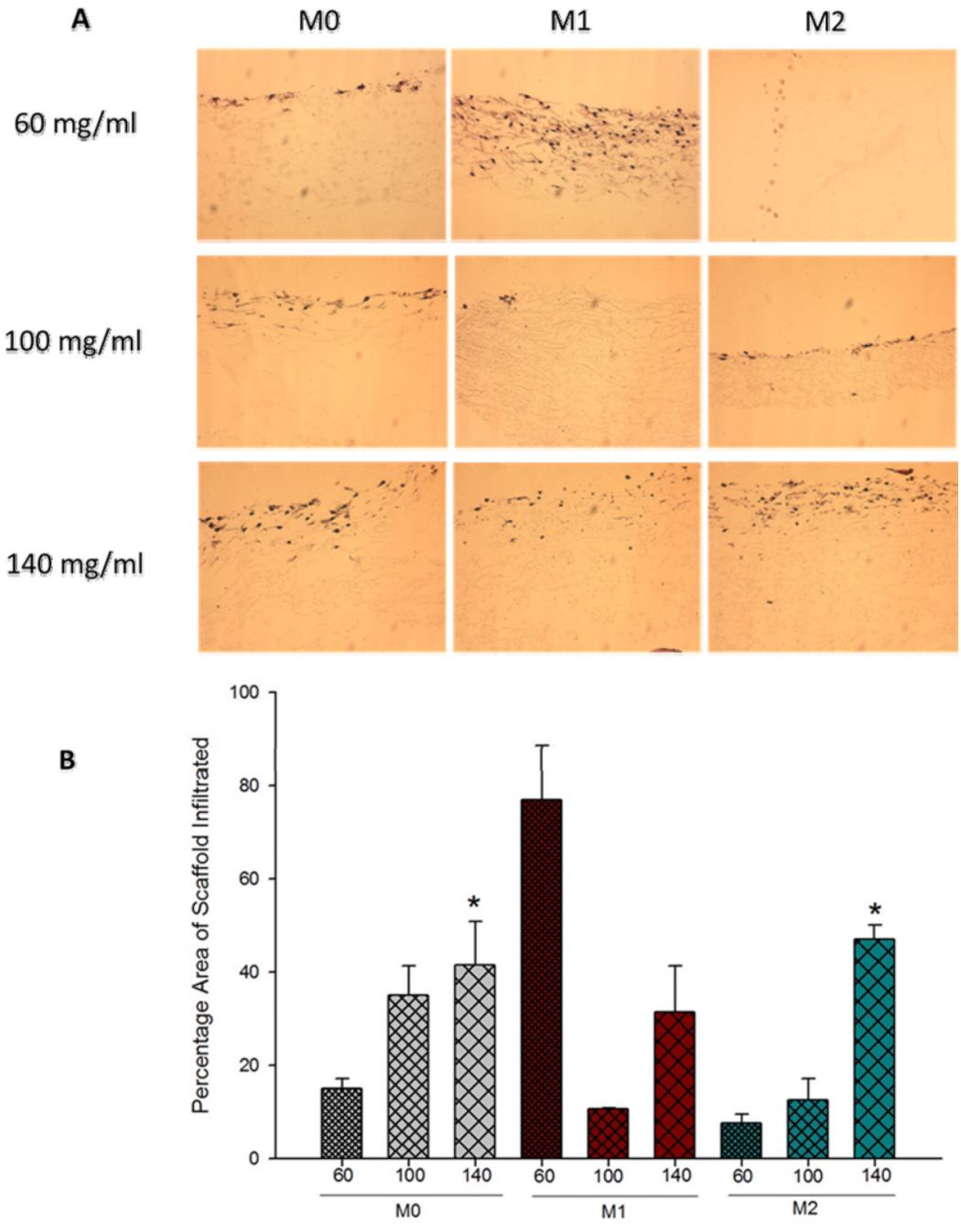

Figure 4.

(A) Histological evaluation of BMMΦ infiltration into the fibrous structures of PDO. (B) Quantification of BMMΦ infiltration into the fibrous structures of PDO.

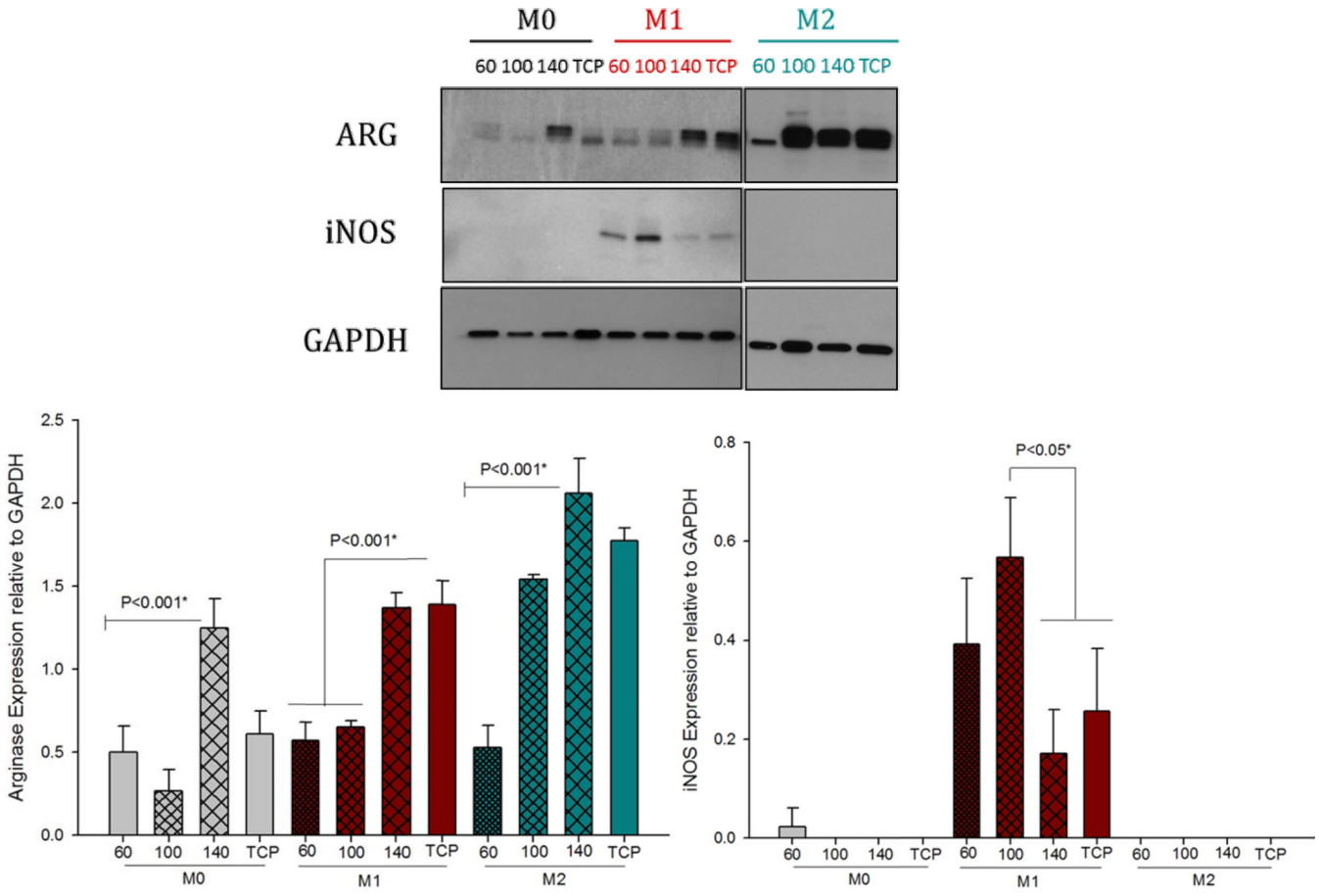

Figure 5.
Arginase and iNOS expression by BMMΦs (M0, M1 and M2) cultured on electrospun PDO scaffolds on Day 1.

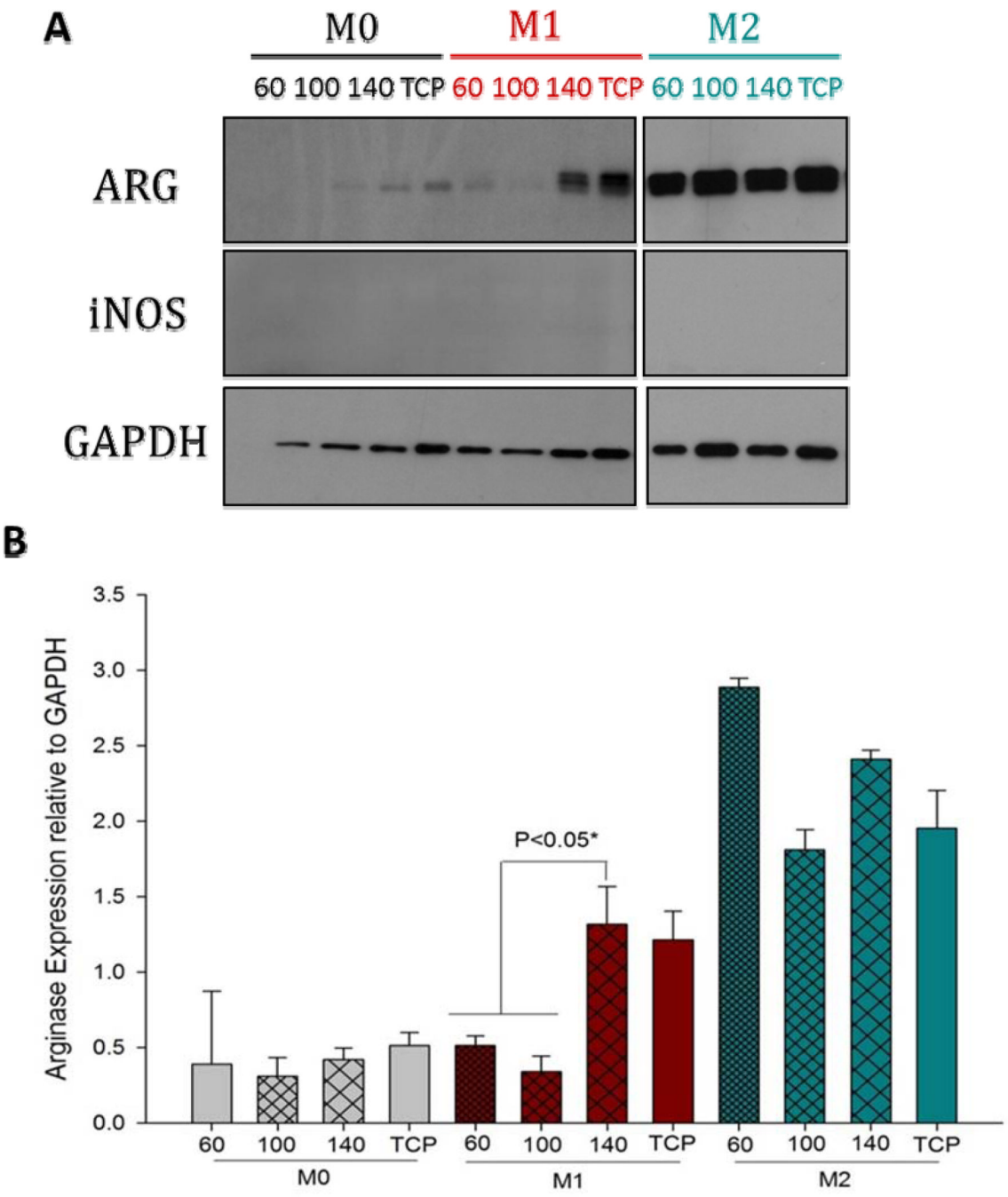

Figure 6.
Arginase and iNOS expression by BMMΦs (M0, M1 and M2) cultured on electrospun PDO scaffolds on Day 3.

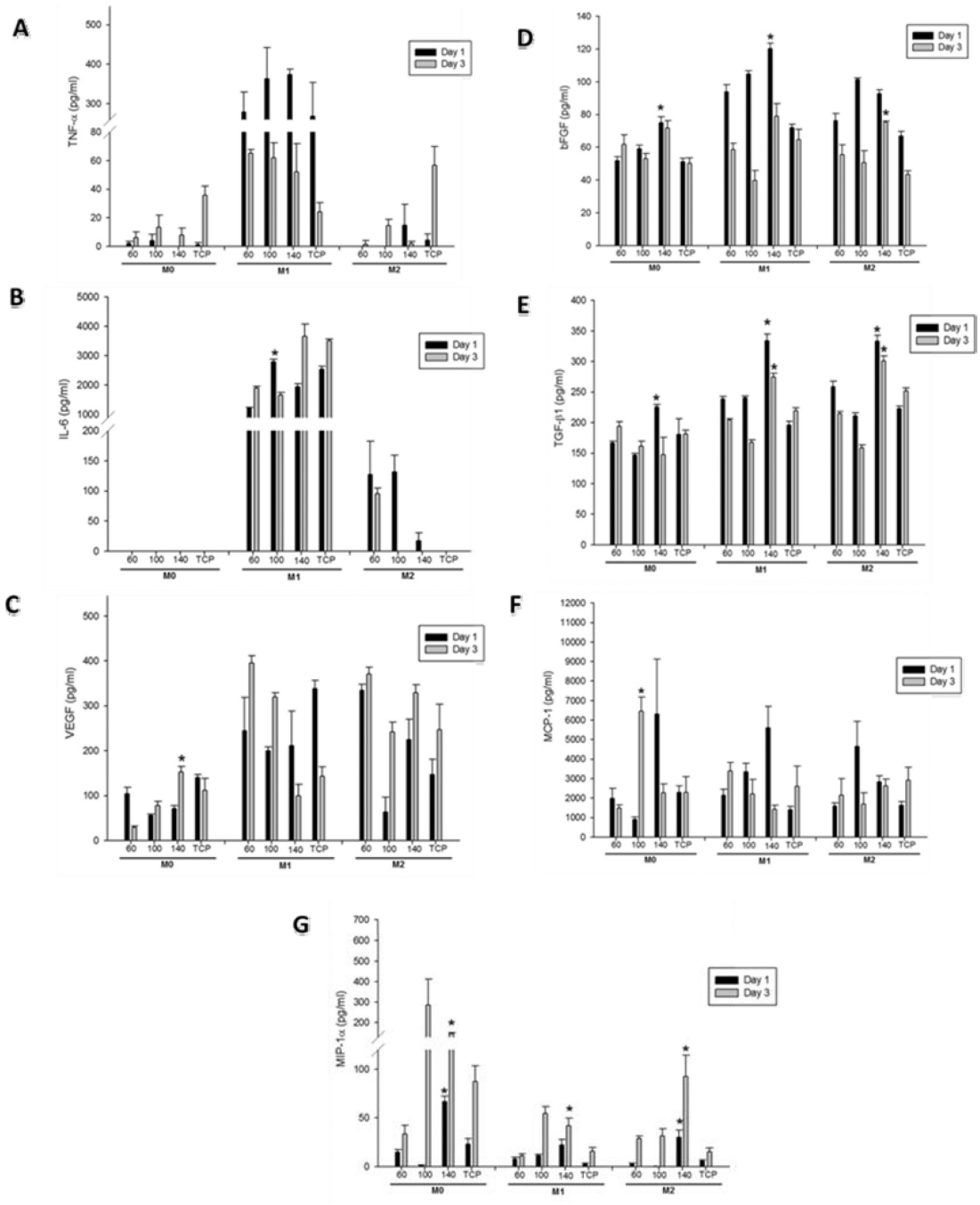

Figure 7.

Quantification of (A) TNF-α, (B) IL-6, (C) VEGF, (D) bFGF, (E) TGF-β1, (F) MCP-1, (G) MIP-1α, levels released by BMMΦs cultured on electrospun PDO on Day 1 and 3.

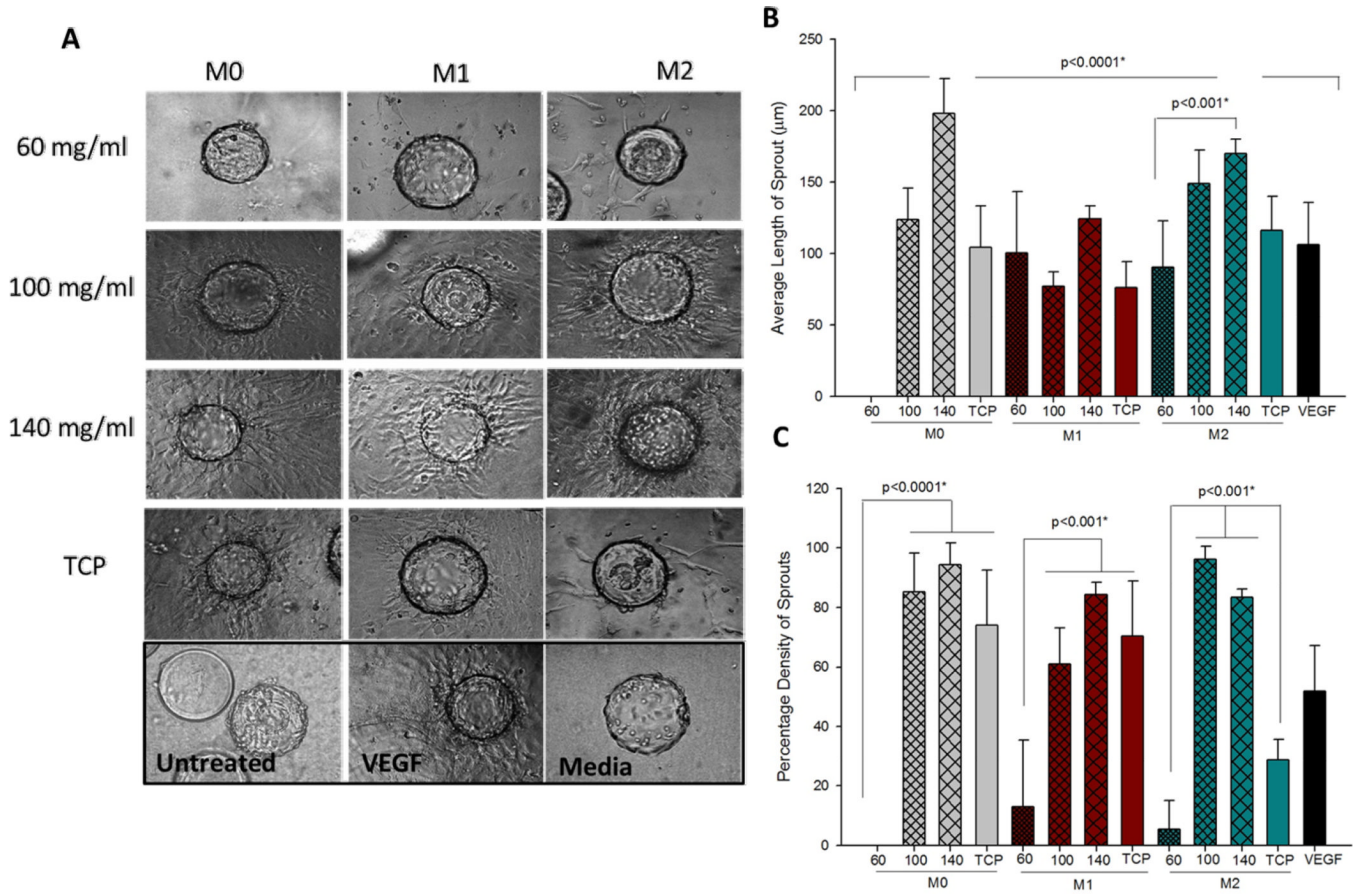

Figure 8.

(A) Sprouting from endothelial cell coated beads in response to conditioned media from BMMΦ and PDO interaction (magnification 10×). (B) Quantification of average length of sprout. (C) quantification of percentage density of sprout.

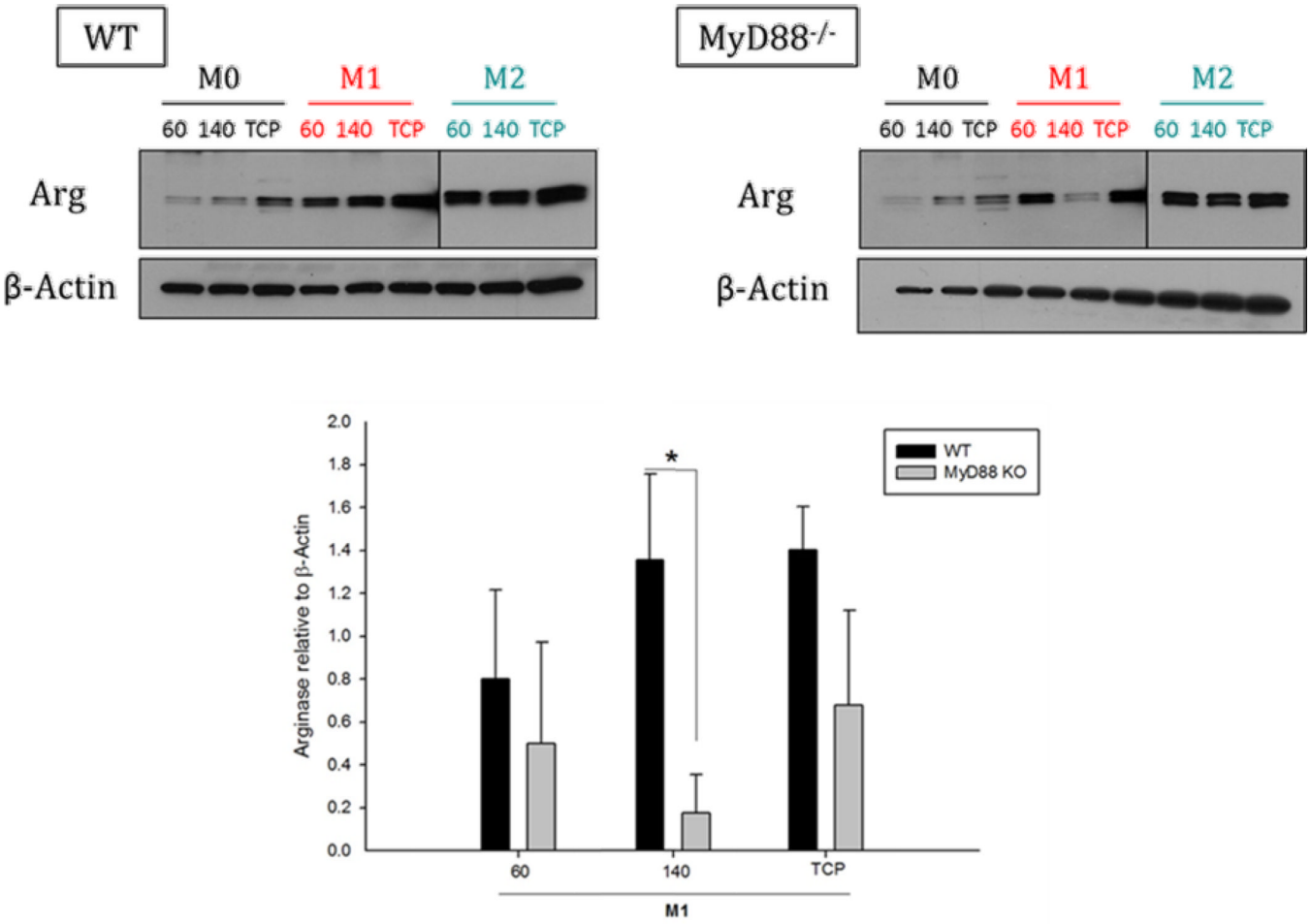

Figure 9.
Role of MyD88 in signaling of BMMΦ on PDO scaffolds (60 and 140 mg/ml).

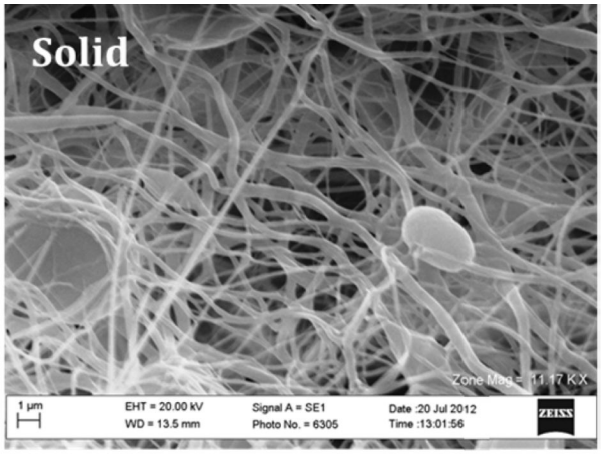

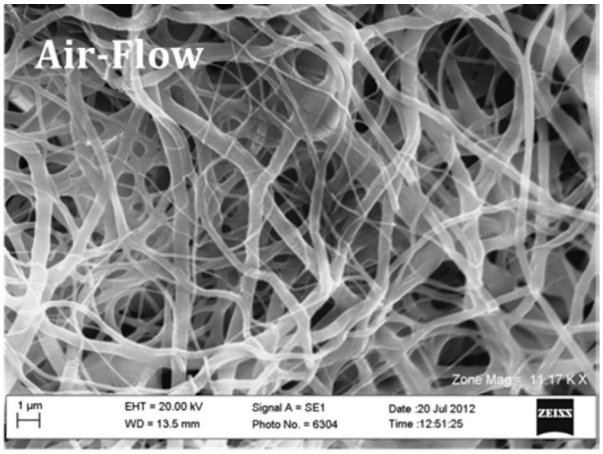

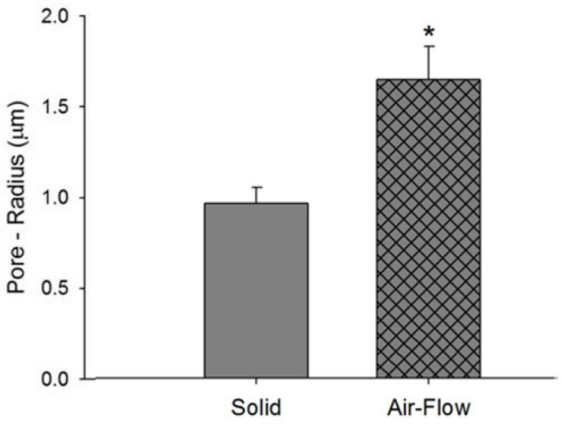

60 mg/ml scaffold	Fiber Diameter (µm)	Porosity (%)	Surface area to volume ratio
Solid Mandrel	0.35 ± 0.126	69.3 ± 2.3	11.43
Air- Flow Mandrel	0.354 ± 0.146	80.4 ± 1.95	11.3

Figure 10.
Comparison of 60 mg/ml PDO scaffolds electrospun on the solid vs. air flow impedance mandrel. The asterisk '*' indicates a statistical difference between the 60 mg/ml and the 140 mg/ml scaffold.

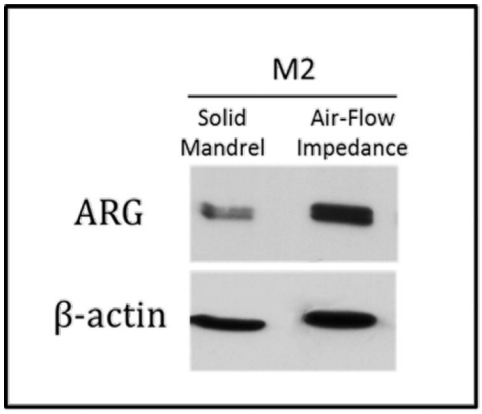

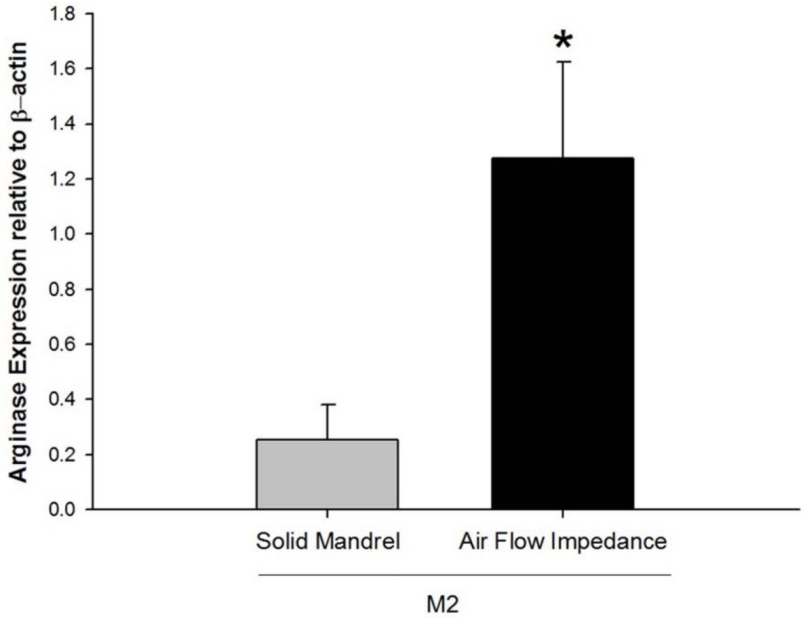

Figure 11.

Arginase expression by M2s on 60 mg/ml scaffold electrospun on solid vs. air flow impedance mandrel. The asterisk '*' indicates a statistical difference between the 60 mg/ml and the 140 mg/ml scaffold.

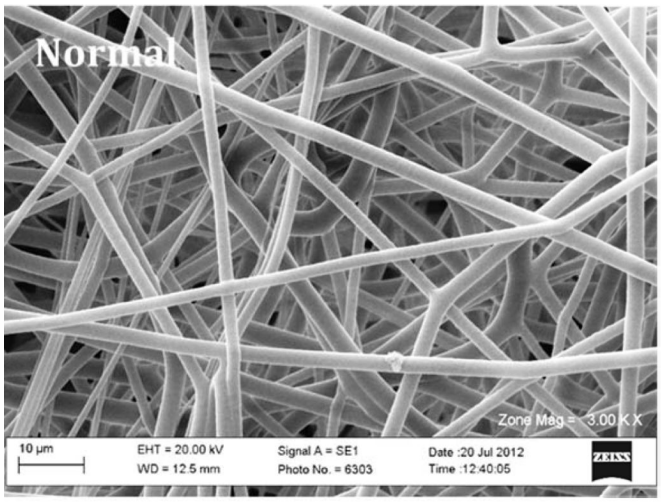

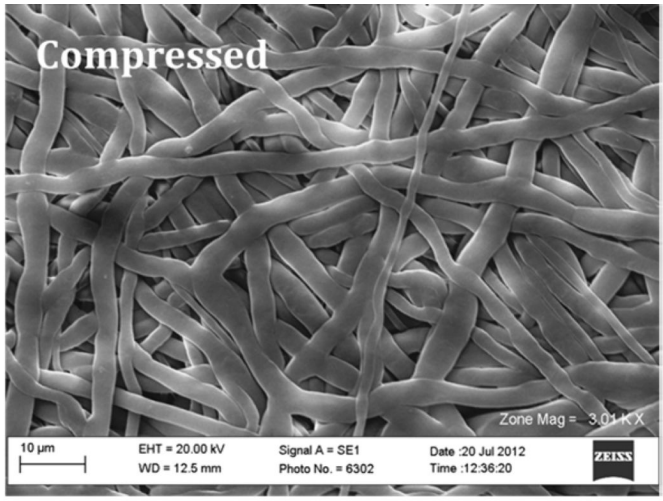

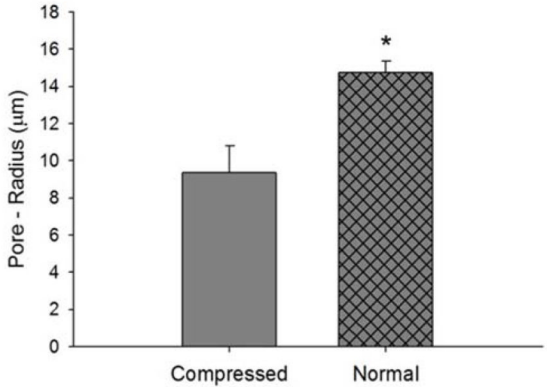

140 mg/ml scaffold	Fiber Diameter (µm)	Porosity (%)	Surface area to volume ratio
Normal	2.8 ± 0.5	82.67 ± 0.7	1.428
Compressed	2.92 ± 1.04	75.52 ± 2.98	1.54

Figure 12.
Comparison of Normal vs. Compressed 140 mg/ml PDO scaffold. The asterisk '*' indicates a statistical difference between the 60 mg/ml and the 140 mg/ml scaffold.

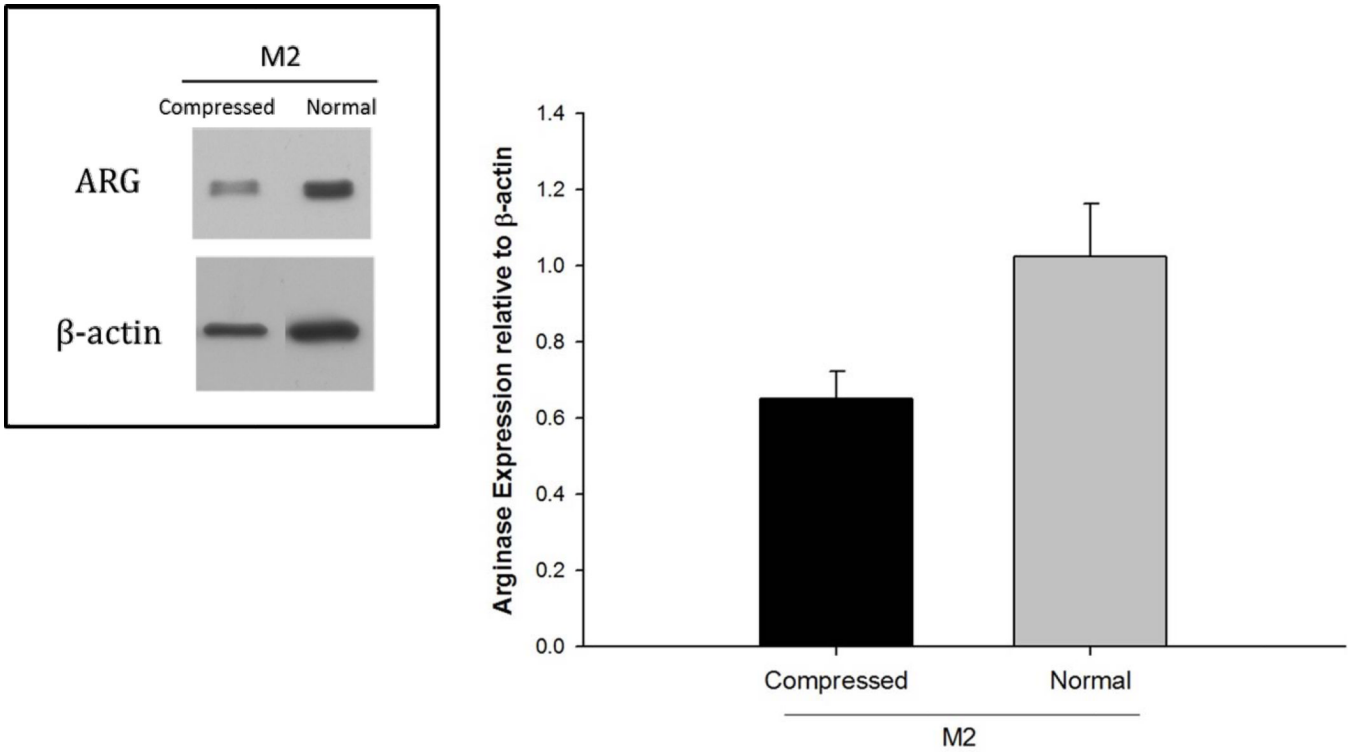

Figure 13.
Expression of Arg1 by M2s on normal and compressed 140 mg/ml PDO scaffolds.